Scaling and flow dependencies over forward-facing steps

Anthony Graziani, Marc Lippert, David Uystepruyst, Laurent Keirsbulck

Scaling and flow dependencies over forward-facing steps

A. Graziani[a,b], M.Lippert[a], D.Uystepruyst[a], L.Keirsbulck[a]

[a]Lamih Umr *8201, F-59313, Valenciennes, France*
[b]*Institut de Recherche Technologique* Railenium, *F-59308, Famars, France*

Abstract

In the present paper, the structure of the mean separation bubbles upstream and downstream of a parametric forward-facing step (Ffs) is experimentally studied over a Reynolds numbers range of Re_h = 110670 – 412000, based on the step height and the free stream velocity. An array of 20 pressure sensors located on the front and on the top sides of the step were flush mounted for capturing the wall pressure fluctuations. Classical Piv was used to investigate the flow field topology and to extract key features. The main interest of this study is to discuss about the parameters affecting the reattachment length and the pressure statistics. A detailled analysis and comparison with the literature of the present study permitted to identify the most important flow quantities influencing the overall dynamics. Different sets of data with various Reynolds numbers, heights to boundary layer thicknesses h/δ, and constriction ratios C_R, have been compared and considered exhaustively. The wall pressures space-time correlations and convection velocities of the large-scale structures downstream the step are highlighted. A focus on the spectral behavior of the unsteady pressure footprint inside the recirculation region of he top side have also been investigated in order deeply understand the unsteady processes described in the litterature. Results demostrate the existance of a convective instability process and a flapping phenomenon of the shear-layer contributing to the separated flow arrangement.

Keywords: Scaling, forward facing step, parametric study, Piv, instabilities, wall pressure measurements.

1. Introduction

Turbulent flow separation occurs in several industry applications, e.g., ground vehicules, planes or internal flow (heat exchangers). The investigation of the flow field over such complex geometries has been a challenge in fluid mechanics mainly due to the non-linear behavior induced by the recirculation regions. For this reason, in practice, simplified academical configurations are generally studied to better understand the flow dynamic mechanisms occurring in such flows. Separated boundary layer due to an adverse pressure gradient, flow over backward facing step and cavities are the most studied. The relative simplicity of these configurations permit to highlight some unsteady phenomena clearly associated to separated flows, such as the low frequency behavior similar to a breathing evolution of the recirculation bubble ([17], [8]). Other classical phenomena, with higher frequency, are also observed, for instance Kelvin-Helmholtz oscillation of the shear-layer and large scale vortices shedding [27]. Separated and reattached flows have received extensive attention in the past decades since the modulation of their instabilities can influence drag behavior ([22]) or noise generation ([1]). However, for industrial geometries, commonly encountered in automotive and aerospace industries, the need of more complex academical geometries is required. In this framework, the forward-facing step (Ffs) is a particularly interesting configuration to analyzed the inter-relations between the two recirculation regions before and after the edge of the forward-facing step. Generally, flow over Ffs is divided into three major regions: upstream, downstream and redevelopment. The upstream one is created by an adverse pressure gradient close to the step surface, reattaching on the front side and interacting with the free stream flow. The second separation occurs at the leading edge and extends downstream. Previous studies have shown that the downstream reattachment length x_r depends on a number of parameter including the step length L, width w and the ratio between the height and the incoming boundary layer thicknes, h/δ ([7],[6], [12]). Bergeles and Athanassiadis [4] showed that the flow around surface-mounted obstacles depends on the step length when $L < 4h$, but for models longer than this value, the position of the reattachment point of the downstream recirculating region remains almost

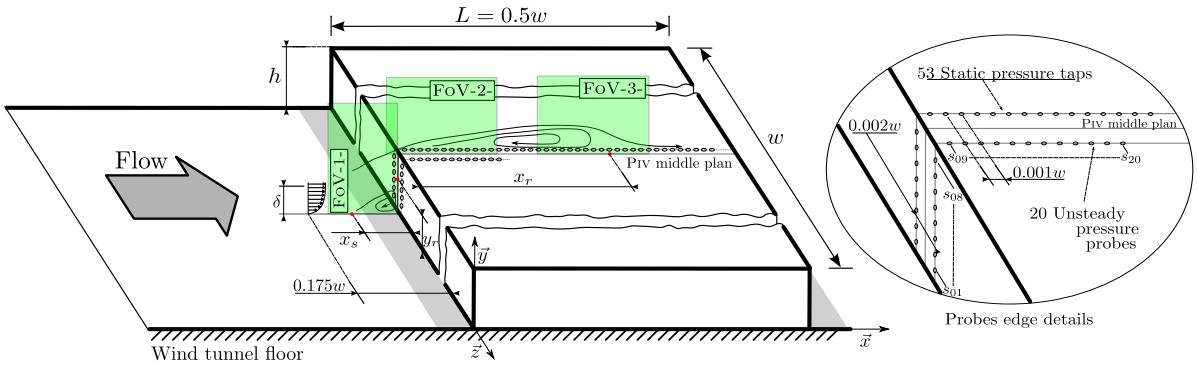

Figure 1: Flow configuration and model instrumentation

constant. In the same way, authors demonstrated that $w > 9$ is requiered to comfort the two-dimensional behavior of the flow. It is well known that the h/δ ratio and the Reynolds number have significant effects on the reattachment length and turbulent statistics [2], but although the Fps turbulent flows have been studied in the past, no consensus about these dependencies has been clearly reported in the literature. The constriction ratio $C_R = S_d/S_u$ (where S_u and S_d are respectively the test section upstream and downstream from the step corner) seems to also have a significant effect on the separated flow fields, as reported by Lanzerstorfer and Kuhlmann [18]. Sherry *et al.* ([24], [25]) concluded that the discrepancy observed in the literature is maily caused by upstream flow conditions combined with body geometry effects, but also due to other parameters. Furthermore, in contrast to the large number of prior studies of turbulent flows, comprehension of flow dynamic close to the leading edge is relatively limited. Concerning the instability processes occurring in the forward-facing configurations, Farabee and Casarella [10] and more recently Camussi *et al.* [5] have shown the existence of frequency peaks in the pressure spectra inside and outside of the separation region. The spectra in the downstream region exhibits a dual mode with high- and low-frequency broad band peaks, until a distance $x/h \approx 0.5$ from the elading edge. Beyond this distance, all the spectra exhibit a single peak close to $f.h/U_\infty = 0.15 - 0.2$. Similar observation are also obtained by Awasthi *et al.* [2]. All the experimental studies cited above were conducted on various configurations including three dimensional cases, and were onyl focused in the global separated flow structures. It appears that no detailed investigation of separated and reattached flows, on the leading edge region, has been made to better describe instabilities formation and evolution. Moreover, most of them underline the difficulty to validate their results with the literature mainly due to the numerous parameters affecting the key flow features. Thus, the objective of this study is first to investigate the parameters dependencies of the separated flow over two-dimensional rectangular step, and secondly to identify the instabilities involved in the downstream separation area, with a particular attention to the edge region. The data obtained could also be helpful in further numerical simulations for the validation of turbulence models.

This paper is organized as follows: Sect. 2 presents the experimental apparatus with a description of the forward-facing step configuration and the measurement setup. Sect. 3 is divided in two subsections. The first one is devoted to the description of the mean-flow features and extraction of the main parameters and conditions. The second one provides a discussion on the dependencies of some parameters, including the reattachment lengths, pressure statistics and spectrum with regards to the constriction ratios C_R, h/δ ratios and Reynolds number. All of the present data was validated and compared to previous experimental and numerical results. Finally a conclusion is given in Sect. 4.

2. Experimental apparatus

2.1. Forward-facing step configuration

Experiments took place in the optically accessible Lamih closed-loop wind tunnel composed by a 2m×2m×10m test vein. The air is conditioned in a

Table 1: Averaged flow parameters.

Studies/parameters	upstream			step						
	U_∞ [m/s]	δ (mm)	Re_δ	h (mm)	CR	h/δ	Re_h	$y_r^\star$	$x_r^\star$	Symbols
+ Present experiment	10	81.9	54625	166	0.92	2.026	110670	0.584	3.22	◆
				186	0.91	2.270	124000	0.575	3.30	◆
				206	0.90	2.514	137330	0.560	3.35	◇
	20	74.2	98980	166	0.92	2.236	221340	0.566	3.42	▼
				186	0.91	2.506	248000	0.554	3.44	▼
				206	0.90	2.775	274660	0.540	3.47	▽
	30	70.9	141795	166	0.92	2.341	331910	0.533	3.49	■
				186	0.91	2.623	372000	0.553	3.52	■
				206	0.90	2.905	412000	0.531	3.55	□
	U_∞ [m/s]	δ (mm)	Re_δ	h (mm)	CR	h/δ	Re_h	$x_s^\star$	$x_r^\star$	Symbols
★ Awasthi *et al.* (2014) [2]	30	97.0	177000	14.6	0.99	0.151	26600	-1.9	3.6	◀
				58.3	0.97	0.601	106000	-	4.1	◁
	60	95.0	346000	14.6	0.99	0.154	53200	-1.7	3.7	▶
				58.3	0.97	0.615	213000	-1.5	4.2	▷
● Largeau & Moriniere (2007) [19]	40	8.0	21330	30	0.93	3.846	80000	-1.27	3.5	
				40	0.91	5.000	106670	-1.25	3.62	
				50	0.89	6.250	166670	-1.22	3.75	

settling chamber to minimize free stream turbulence through a nozzle with a 6.25 contraction ratio. The facility can operates in a velocity range from 0.5 to 60m/s with a low inlet turbulent intensity (0.6 % of free stream velocity). More details about the facility can be found in Keirsbulck *et al.* [16]. A scheme of the present forward-facing step configuration is given in Fig. 1. The model is mounted on the side wall of the test section at 4m from the nozzle end, it extends all along the spamwaise direction, w = 2000mm, to guarantee a two-dimensional separated flow configuration. To study the influence of the model geometry over the separated flow, three different forward-facing step heights h 166mm, 186mm and 206mm are investigated. These heights give rise to constriction ratios CR in the range from 0.897 to 0.917. The dimensionless[1] spanwise length range, corresponding to these step heights, is $w^\star$=9.7-12 sufficiently high to neglect wall effects [4]. The length of the step L is 1000mm (0.5w), with $L^\star$ between 4.85 and 6.02, assuming Bergeles & Athanassiadis [4] statement, which recommended $L^\star > 4$ to insure that the downstream recirculating region do not change with this parameter. The free stream flow velocity and averaged incoming boundary layer profiles were measured with a Pitot tube at 350mm (0.175w) upstream of the step edge. Three free stream velocities, U_∞ = 10, 20 and 30 m/s, were experimentally investigated for each flow configuration. The origin of the co-ordinate system is located at the step base. The abscissa axis x, represents the streamwise flow direction, the ordinate axis y is the normal direction to the flow, the third axis z corresponds to the spanwise or cross-stream flow. The ensemble-averaged and fluctuating horizontal and vertical velocity components are denoted by U, V , u and v respectively. The ensemble-averaged and fluctuating pressure are denoted by P and p. The two Reynolds numbers considered hereafter are based on the free stream velocity and the boundary layer thickness Re_δ, and step height Re_h.

[1] $\star$ symbol denotes the step height dimensionless value

2.2. *Surface-pressure and velocity measurements*

A first set of 53 static pressure taps has been evenly distributed over the forward-facing step in the free stream direction at 20mm (0.001w) spanwise from the middle plan of the model and separated 20mm from each others. A total of 45 taps are located on the top side and 8 on the front side of the step as shown in Fig. 1. In addition, the wall-pressure signature, induced by the convection of instabilities, is measured using 20 flush-mounted commercial KULITE-XCP-062 sensors, 8 of them are located on the step front side and 12 on the top side, located parallel to the static pressure taps but in a negative spanwise direction, (-20 mm) from the middle plan, to avoid interferances with the PIV laser sheet. Pressure time histories were recovered using 2 commercial DEWESOFT-STG+ acquisition units providing auto-calibration, A/D conversion and filtering. The calibration curves of the transducers were determined by the manufacturer and directly used by the acquisition system. The sample frequency of the sensors was set at 10 kHz to capture the overall dynamic of the flow at the highest Reynolds number. The measurement noise was removed by applying a 8^{th} order Bessel filter with cut frequency f_c = 3 kHz. A total acquisition time of 5

minutes was made for all cases to reach statistical convergence. The velocity flow fields were obtained using a standard two-component Tsi particle image velocimetry (Piv) system. The flow is seeded with 10 μm olive oil particles using a jet atomizer upstream of the stagnation chamber. The system consists in a double-pulse Nd:YaG laser system generating a 532 nm light sheet located on the model centerline, which enlight the tracers at a sample frequency $f_{\text{Piv}} = 7Hz$. Their displacement were captured in three different locations using 2048×2048 pixels Powerview cameras, coupled with two 85mm (FoV-1-, FoV-2-) and one 50mm (FoV-3-) optical lenses. The velocity vector fields were recovered using a direct cross-correlation algorithm on a rectangular grid composed with 50% overlapped 16×16 $pixels^2$ interrogation boxes, which generates a final spatial resolution $\Delta x = \Delta y \simeq 1mm$. As a post-processing, a low-pass filter was applied to remove measurement noises. The images treatment was performed using the commercial software Insight 4G distributed by Tsi. For every test cases, 2000 double-frame pictures were recorded to assure velocity field statistic convergence. These velocity fields were used in particular to obtain two different points. The first reattachment point y_r situated at the upstream recirculation bubble, front step side. The reattachment point x_r of the second recirculation bubble located downstream the step edge. Both lenghts are shown in Fig. 1.

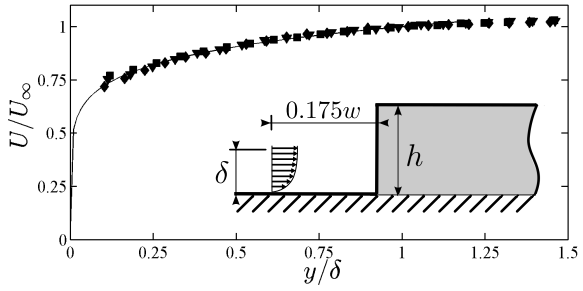

Figure 2: Dimensionless boundary layer profiles against the wall normal distance for U_∞=10, 20 and 30m/s. Solid line denotes the turbulent $\frac{1}{7}$ power law.

3. Results

3.1. Mean flow parameters and features

To define the average flow characteristics, the boundary layer is firstly extracted from Pitot tube velocity profiles at a distance of 0.175w upstream of the step for the three velocities studied. All velocity profiles, plotted in Fig. 2, were correlated with the classical turbulent $(1/7)^{th}$ power law. The boundary layer thickness, δ, the associated Reynolds numbers and the h/δ ratios are computed and reported in Tab. 1. Piv datas from the FoV-1- and -3- are also analyzed in order to determine the key parameters of the recirculation bubbles, i.e. x_r and y_r. The velocity average flow fields, for all the Reynolds numbers, show a classical flow structure. A long separation area beginning at the edge of the step until the reattachment point and a second one before the step at the bottom edge are clearly seen. The reattachment and separation points are extracted from the Piv velocity fields by tracking the position where the near-wall velocity reaches zero. An example of the streamlines flow fields and the near-wall velocity profiles are given in Fig. 3 and 4. The extracted reattachment lengths are reported in Tab. 1 for all the studied cases with the mean-flow parameters of Awasthi *et*

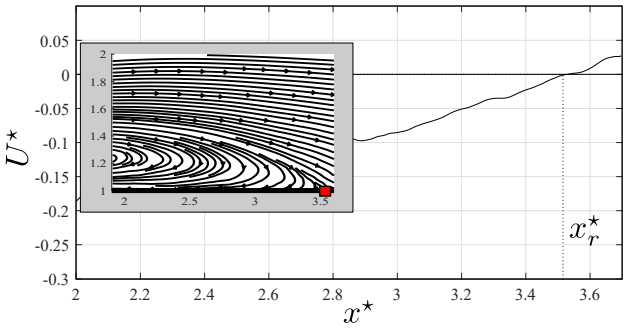

Figure 3: Streamlines and associated wall-velocity profile (extracted from the Piv field at a distance $y^\star$=0.01 from the wall) downstream the step edge for Re_δ = 141795 and h/δ = 2.623. Red square symbol denotes the second reattachment point $x_r^\star$.

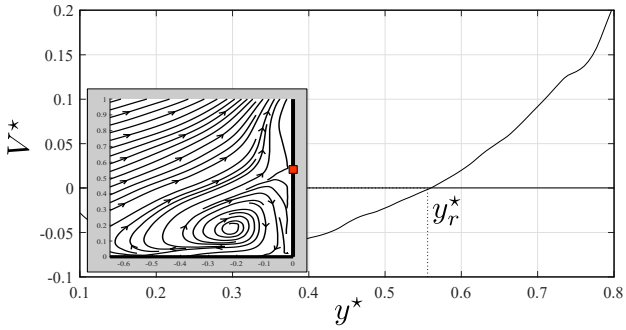

Figure 4: Streamlines and associated wall-velocity profile (extracted from the Piv field at a distance $x^\star$=0.01 from the wall) upstream the step edge for Re_δ = 141795 and h/δ = 2.623. Red square symbol denotes the first reattachment point $y_r^\star$.

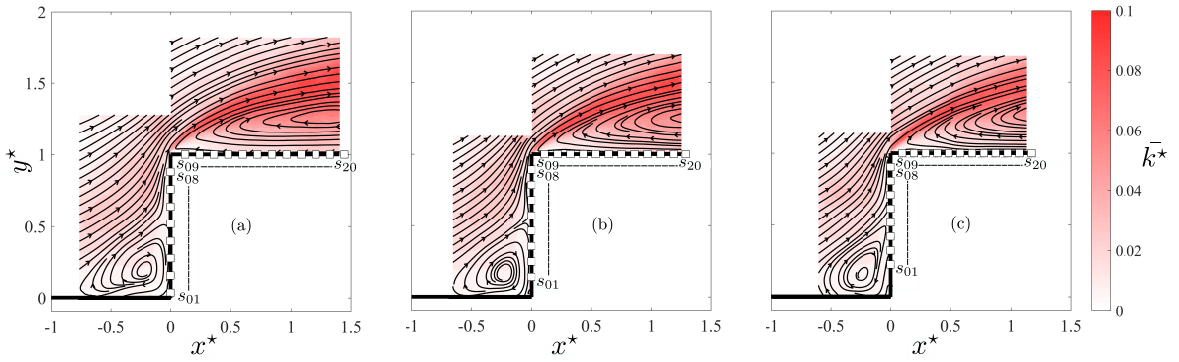

Figure 5: Contour maps of partial averaged turbulent kinetic energy superimpose with streamlines obtained at Re_δ=98980 for (a) h/δ =2.236, (b) 2.506 and (c) 2.775.

Table 2: References and associated parameters.

Studies/parameters	Cr	$Re_h \times 10^{-3}$	h/δ	$x_r{}^\star$
▶ Bergeles *et al.* [4]	0.91	27	2.08	3.75
▲ Sherry *et al.* [25]	0.95	1.50 - 7.50	0.40	2.4 - 3.9
▲	0.93	2.80-14.0	0.80	1.9-3.1
△	0.92	3.80-19.0	1.20	2.8-3.9
◀ Ji and Wang [15]	0.91	6.48	0.13	2.16
	0.91	25.92	0.53	2.93
○ Gasset *et al.* [11]	1.00	50	1.43	5.00
● Leclercq *et al.* [20]	0.90	170	1.43	3.20

al. [2] and Largeau and Moriniere [19]. For the same Reynolds number based on the boundary layer thickness Re_δ, the effect of h/δ ratio on the flow features is significant as also observed in the literature ([2], [19]). A way to quantify this effect is through the partial averaged turbulent kinetic energy ($\overline{k^\star} = (\overline{u^2} + \overline{v^2})/2$) and associated streamlines obtained in the region nearby the obstacle, at Re_δ = 98980 for three different h/δ ratio (Fig. 5). The streamlines permit to distinguish the main flow pattern with two recirculation region. The first one, at the bottom of the step, separates upstream (outside the FoV-1-FRAM) and reattaches on the front face; the second one, more massive, starts from the leading edge in FoV-2- and reattaches on FoV-3-. Interaction between the recirculating regions and the external flow occurs through the free shear mixing region. From the streamlines pattern, the first reattachment point y_r (front face) impignes the wall at approximatly half of the step height, as reported in Tab. 1, regardless of the Reynolds number and h/δ ratio. The shape of the first recirculation bubble, at the front of the step, changes when the h/δ ratio increases and it center moves upstream as previously reported in the literature ([19], [2], [3], [21]). An increase of h/δ also affects the massive separation region (top face), leading to a rise of the reattachment point x_r and a displacement of the center of the bubble in the free-stream direction. Same observation can be seen for the two other Re_δ studied. It is also noticed that the partial averaged turbulent kinetic energy intensity is maximum inside the downstream shear layer.

3.2. *Scaling and parameter dependencies*

A lack of consensus concerning the scaling of the reattachment length downstream of the step is clearly seen. Most of the results obtained from previous studies showed a large scattering highlighting a flow dependency to external and internal parameters ([10], [11], [26], [14], [23]). Sherry *et al.* ([24], [25]) have shown that the x_r variation depends on the Reynolds numbers and the ratios between the step height and the boundary layer thickness h/δ. Past results showed a strong dependency to the Reynolds number until a $Re_c \simeq$ 8500, above this critical value, the dependency becomes lesser. However, the authors underlined that the offset observed between the results at the same Reynolds number is due to a combined effect of the upstream flow conditions, principally the boundary layer thickness and body geometry effects. In order to analyze in details the Re_h and h/δ effects on x_r, previous and present reattachment lengths are plotted and compared in Fig. 6. Only the data with dimensionless spanwise, $w^\star$ and step length, $L^\star$ higher that 9 and 4 respectively, was selected to avoid geometrical under dimensioning effects. Tab. 2 reports authors references that are being compared. Fig. 6 shows, as previously mentioned by Sherry *et al.*, a strong Reynolds effect untill Re_h = 8500. For

$Re_h > 8500$, all the data set are included ina wide constant region (denoted by a gray area in Fig. 6). Nevertheless, the data are scattered and showed no clear dependency against h/δ collapsing quite well to a single constant line when plotted against Re_h. Thus, the boundary layer thickness doesn't appear to be the dominating parameter of the average flow topology. Another important quantity seems to be the constriction ratio C_R. While the h/δ ratio tends to decrease the reattachment length, the constriction ratio tends to have an opposite behavior. The x_r shift, observed in the three data sets of Sherry *et al.* [24], can be explained as a variation of the flow blockage caused by the step, even if $1 - C_R$ is less than 10%.

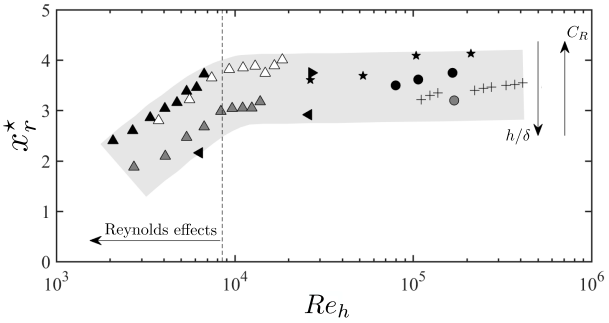

Figure 6: Reattachment lengths against Reynolds numbers. + present data, ▲ ▲ △ Sherry *et al.* [25], ◀ Ji and Wang [15], ● Leclercq *et al.* [20], ▶ Bergeles *et al.* [4], ★ Awasthi *et al.* [2], ● Largeau & Moriniere [19].

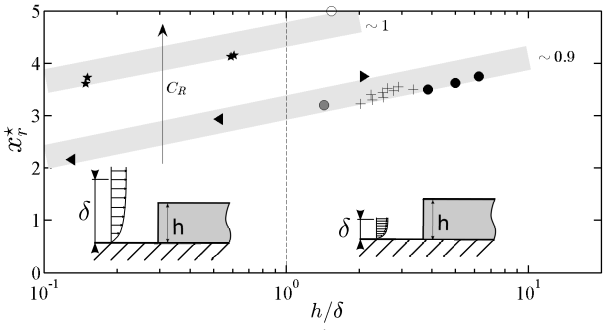

Figure 7: Reattachment lengths against h/δ. Symbols are the same as in Fig. 6

To clarify the parameter dependency influencing the x_r evolution, the reattachment length against the h/δ ratio was plotted in Fig. 7 in a semi-log representation for $Re_h > 8500$ to neglect the Reynolds effects. Following this representation, it is possible to observe the effect of the parameters h/δ and C_R independently. Data from two different constriction ratios, arround 0.9 and 1, are plotted against h/δ and denoted by gray lines. The main observation is that the x_r evolution is driven by the h/δ ratio and follows a logarithmic behavior, shifted by the modification of C_R. Secondly, for a given constriction ratio, the slop of the linear trend seems to varying, depending of the group of scatters observed, as shown for example for $C_R = 0.9$. These conclusions are only partially consistent with the observations of Sherry *et al.* [24] who argue that, for configurations were $h/\delta < 1$, the reattachment length a strong function of Reynolds number and only weakly dependent on h/δ. It is interesting to postulate that the reattachment length evolution may be consistent with a logarithmic distribution of h/δ at Reynolds number higher than 8500. The reattachment length downstream of the step would then be expected to scale as

$$x_r^\star = a.log(h/\delta) + f(C_R) \quad (1)$$

where a could be a function of other parameters, but cannot be identify in the present study completly. As mentioned in the literature, the flow topology upstream of the step is strongly dependent on h/δ and drives the shear mecanism, on the step leading edge, by direct interaction with boundary layer turbulences ($h/\delta < 1$) or free stream flow ($h/\delta > 1$). This variation of velocity, inducing significant reattachment length modifications, is taking into account in the previous scaling formulation by the constriction ratio. The latter returns the blockage effect of the model and enhances the mixing effects within the shear layer.

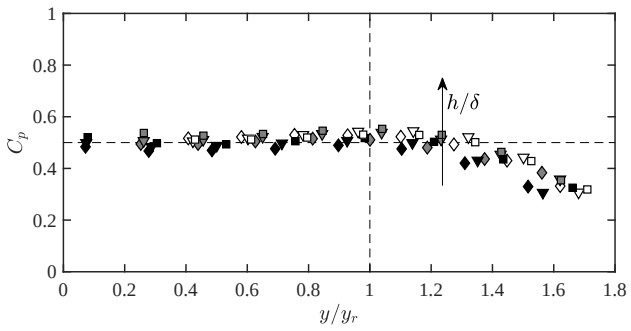

Figure 8: Mean-pressure coefficient distribution against y/y_r over the front side for $Re_\delta = 54625$ (diamond symbols), 98980 (down triangle symbols), 141795 (square symbols) and for various h/δ ratio reported in Tab. 1 as follows; ◆ h/δ =2.026, ◆ 2.270, ◇ 2.514, ▼ 2.236, ▼ 2.506, ▽ 2.775, ■ 2.341, ■ 2.623 and □ 2.905.

We focus now on the wall pressure statistical dependencies along the forward facing step. Fig. 8 shows the evolution of the mean-pressure coefficient over the step front side, $C_p = 2.(P - P_{ref})/(\rho U_\infty^2)$, with P_{ref}

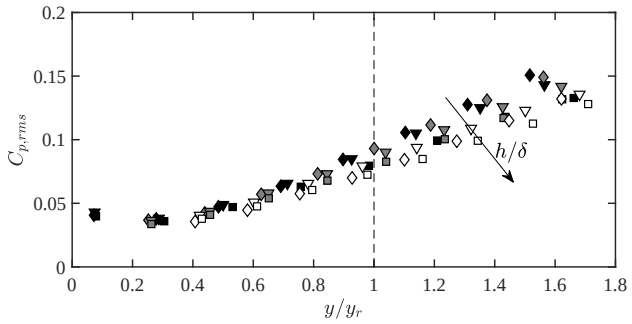

Figure 9: Rms-pressure coefficient distribution against y/y_r over the front side. Symbols are the same as in Fig. 8.

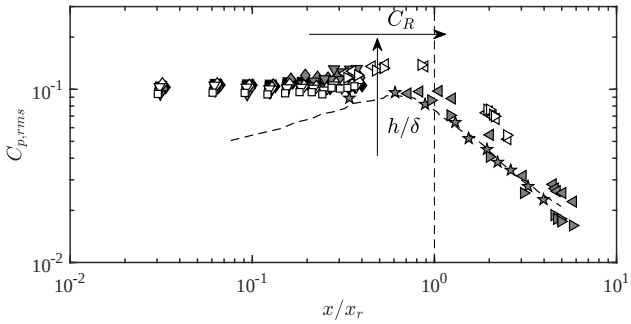

Figure 11: Rms-pressure coefficient distribution against x/x_r along the step top side. Symbols as the same as in Fig. 10. Rms-pressure coefficient are compared with results from ★ Farabee and Casarella [10].

the reference static pressure taken at $x^\star = -6$ for all the Reynolds numbers studied. The global evolution is independent of the Reynolds number, the averaged value of the pressure coefficent is centered arround 0.5 inside the recirculation bubble ($y/y_r < 1$), and tends to decrease to 0.3 outisde this region with a small h/δ effect. This behavior is explained by an acceleration of the fluid flow in the normal direction after the reattachment to the front side. Concerning the associated rms-pressure coefficient, $C_{p,rms} = 2.p_{rms}/(\rho U_\infty^2)$, plotted in Fig. 9, a first constant value of 0.03 from $y/y_r = 0.04$ to 0.4 is observed, following by a monotonous increase up to 0.15 for all cases. The slope of the linear trend denotes a h/δ variation. No Reynolds number effect was observed.

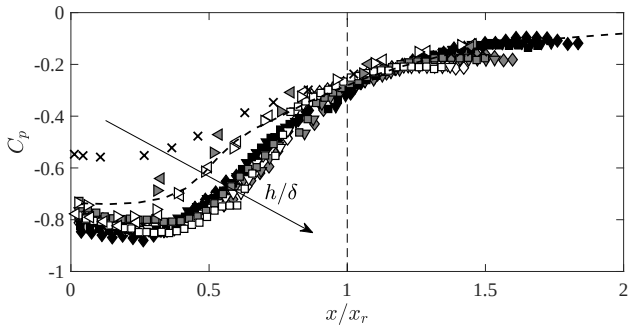

Figure 10: Mean-pressure coefficient distribution against x/x_r along the step top side. Symbols are the same as in Fig. 8. Mean-pressure coefficients were compared with results from × Castro *et al.* [6] for $h/\delta = 0.19$, – – Ji and Wang [15] for $h/\delta = 0.53$ and from Awasthi *et al.* [2] for various h/δ ratio reported in Tab. 1, as follows; ◀ h/δ =0.151, ◁ 0.601, ▶ 0.154, ▷ 0.615.

Fig. 10 shows the evolution of the mean-pressure coefficient along the steps top side. As observed on the front side, no dependency over the Reynolds number is clearly identify. However, a significant h/δ effect is highlighted and corroborated by adding the data set of Ji and Wang [15], Awasthi *et al.* [2] and Castro *et al.* [6] whixh have lower h/δ ratios than the present study. This strong decrease of the mean-pressure coefficient is associated to an increase of the h/δ ratio. The mean-pressure inside the separation bubble appears to be very sensitive to the h/δ ratio, strong variation of the mean-pressure are clearly seen when $h/\delta < 1$, while for $h/\delta > 1$ the pressure evolution reaches a critical minimum value. The rms-pressure coefficient is compared to other authors (Farabee and Casarella [10] and Awasthi *et al.* [2]) in Fig. 11 and shows a typical behavior associated to separated/reattached flows. Farabee and Casarella [10] highlighted that for both backward- and forward- facing step configurations, the reattachment point of the flow is associated to strong pressure fluctuations. These high fluctuations are observed by a rms-pressure coefficient peak close to $0.8x_r$. The position of the peak seems also depend on the constriction ratio and gets closer to the reattachment position as C_R increases. An h/δ effect is also observed, where the peak value is higher for high h/δ.

3.3. Unsteady behavior and shear-layer instabilities

Instantaneous flow fields are now investigated to highlight the shear-layer large scale structures evolution. Three consecutive normalized vorticity snapshot #100, #101 and #102 are shown in Fig. 12 at Re_δ=98980 for h/δ=2.236. Most of the large scale flow structure activities are located in the shear-layer, as previously mention in Fig. 5 by the high level of partial averaged turbulent kinetic energy. Moreover, in addition to the self production of shear-layer vortices, a flapping motion of the shear-layer is clearly visible in the snapshot #100 and #102. The shear-layer moves with a breathing motion, this phenomenon was previously

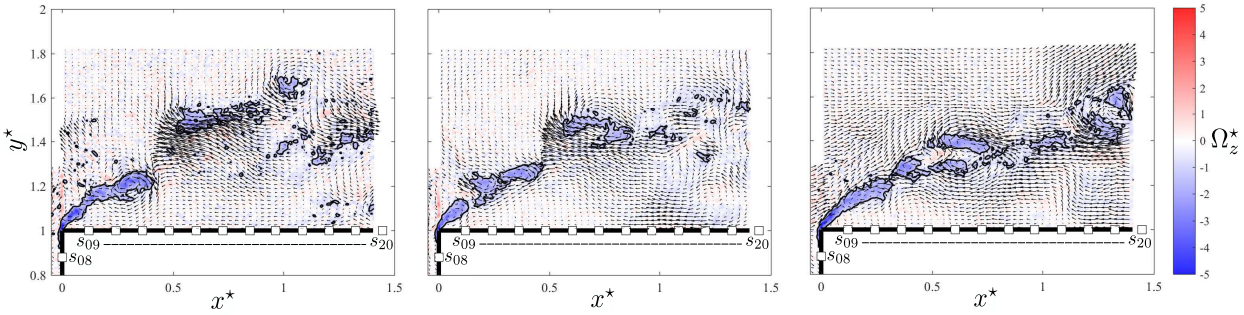

Figure 12: Typical vector maps of the instantaneous velocity field #100, #101 and #102, superimposed on the normalized vorticity, $\Omega_z.h/U_\infty$, distribution at Re_δ=98980 for h/δ=2.236. The instantaneous spatial mean velocity is subtracted to highlight the flow structure.

described by Kiya and Sasaki [17] and Cherry *et al.* [8]. The origin of this unsteady mechanism is still not clearly understood. However, the existence of such phenomenon is observed for some separated flow configurations (backward-facing step [13], blunt flat plate [27], boundary layer or bump configuration with adverse pressure gradient [9]). The flapping frequency in these configurations are generally associated to a dimensionless frequency of $f.x_r/U_\infty = 0.12$. For the forward-facing step flow configuration such dimensionless flapping frequency hasn't been clearly defined in the literature. The final part of this paper will be devoted to the unsteady behavior analysis. Fig. 13 exhibits the space-time contour plots of instantaneous wall pressure fluctuations measured for all the pressure sensorsat $Re_\delta = 54625$ and $h/\delta = 2.514$. The first 8 pressures transducers are located on the front side and the 12 others on the top side. The downstream convective feature, denoted by an inclined contour pattern, is clearly observed. It is well known that the instantaneous negative peaks in wall pressure fluctuations are associated with the passage of large scale vortices. As shown in Fig. 13, for both front and top side of the forward facing step, low frequency motions are observed with an alternative low and high pressure levels. A typical time scale of about $t.U_\infty/h = 20$ is observed and agree well with the flapping phenomena frequency order value.

Fig. 14 and 15 show 3D plots of the pressure fluctuations spectra for all the sensors locations at $Re_\delta = 141795$ for $h/\delta = 2.905$ and 2.341 respectively. On the front side region, an energetic monotonus evolution of the spectra is seen from the bottom of the step to the top. On the top side region strong energetic peaks can be identified for both configurations and divided into two different groups. The first one, denotes by a blue circle symbol in Fig. 14 and 15, can be associated to the flapping motion and is more prominent for a lower h/δ

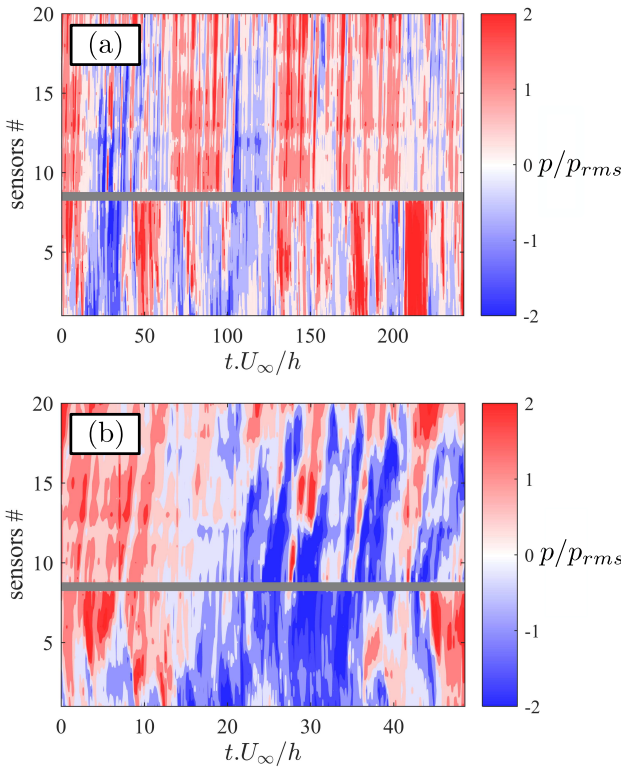

Figure 13: Space-time contour plots of instantaneous wall pressure fluctuations normalized by the rms pressure, p/p_{rms} at $Re_\delta = 54625$ and $h/\delta = 2.514$: (a) long time range to highlight low-frequencies, (b) short time range to better appreciate convectives phenomenon. Gray line denotes the leading edge between the front step and the top step sensors.

ratio as shown in Fig. 15. The second group, denoted by red circles, underlined a convective instability associated to shear-layer oscillation. Similar behaviors were also observed by Farabee and Casarella [10].

In order to analyze in details the behavior of the un-

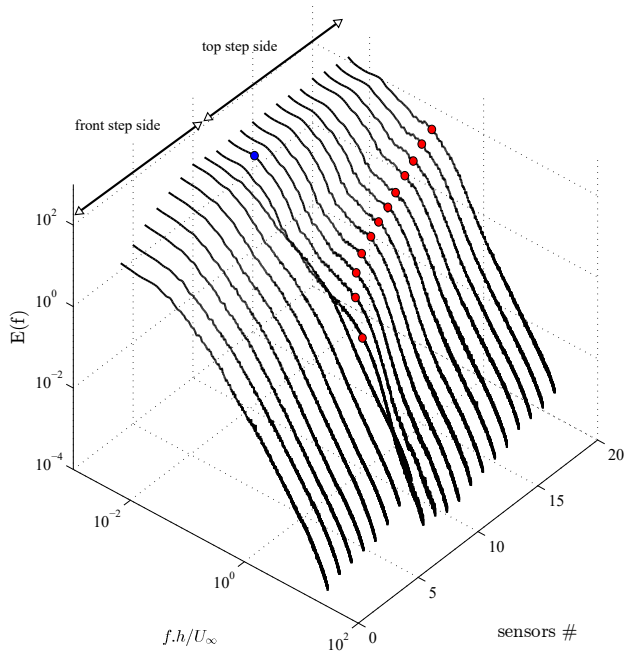

Figure 14: Power spectra of fluctuating wall pressure for different sensors # at Re_δ = 141795 and h/δ = 2.905. Blue circle symbol denotes the constant flapping peak and the red ones denotes the convective instability associate to the oscillation of the shear-layer.

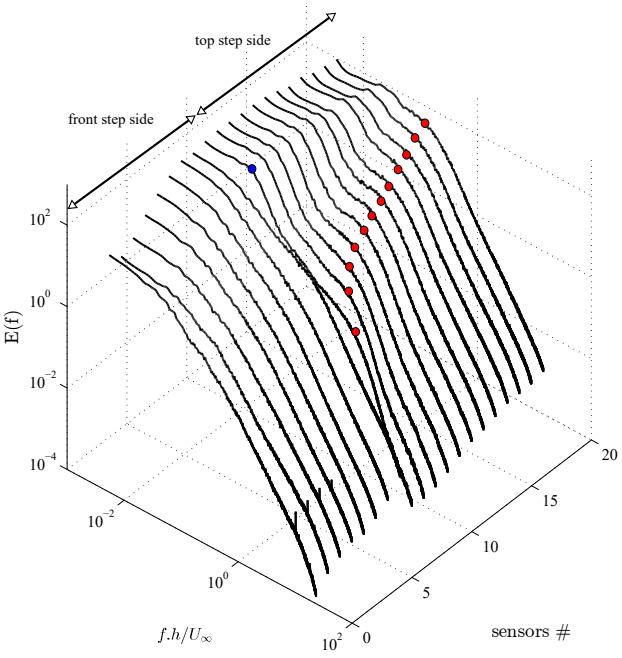

Figure 15: Power spectra of fluctuating wall pressure for different sensors # at Re_δ = 141795 and h/δ = 2.341. Symbols are the same as Fig. 14

steady phenomena the frequencies, for all the flow configurations studied, are extracted and plotted in Fig. 16 and 17. A constant dimensionless frequency of around $f.x_r/U_\infty$ = 0.08 is shown in Fig. 16 independently of h/δ values. Farabee and Casarella [10] observed, close to the step edge, a bimodal spectrum with both low and a high frequency peak. The low frequency peak was obtained at $f.h/U_\infty \approx 0.025$ ($f.x_r/U_\infty \approx 0.085$), and is in agreement with the one obtained in the present study; this peak can be associated to the flapping motion. Fig. 17 exhibits a decrease of the frequency peaks from $f.h/U_\infty \approx 0.8$ at x/x_r = 0.04 to a threshold of 0.15 for $x/x_r \geq 0.5$ for all the studied cases, revealing a convective instability and further asymptotic behavior. Farabee and Casarella [10] and Leclercq *et al.* [20] obtained the same value for the dimensionless frequency peak ($f.h/U_\infty \approx 0.15$). The behavior is Reynolds number independent and shows a very slight h/δ dependency. The convective phenomenon can be associated to the Kelvin-Helmholtz oscillation of the shear-layer, and the asymptotic behavior to the classical shedding of the large scale structures.

The convection velocity of the large scale structures can be computed using the cross-correlations between transducers pairs along the wall and for the different

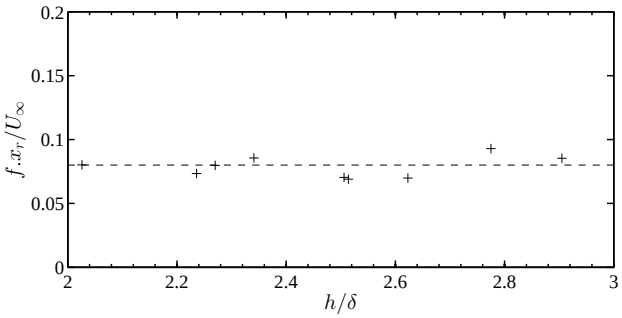

Figure 16: Dimensionless flapping frequency for all the studied cases against the h/δ ratios. Dash line denotes a dimensionless value of 0.08.

cases considered. Results are reported in Fig. 18 and compared with the data of Camussi *et al.* [5] and Largeau and Moriniere [19]. The convection-to-free stream velocity ratio is within the range 0.4-0.8. It decreases from 0.8 to 0.4 for $x^\star < 1$ and increase untill 0.6 at $x^\star = 5$ with no Reynolds number dependency. However, an effect of h/δ parameter can be observed close to the leading edge, and shows a decreasing trend of the convection velocity as the ratio increases. The paramter influence seems to disappear for $x^\star \simeq 0.7$. Present results are in good agreement with the ones obtained in the literature.

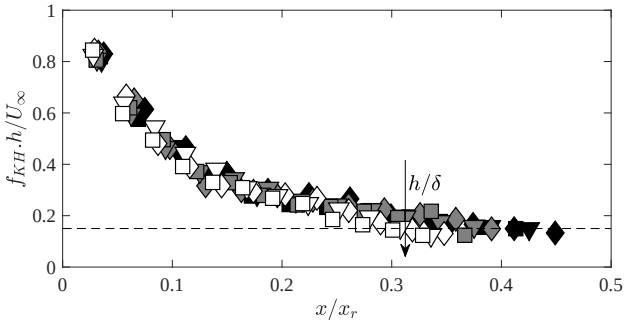

Figure 17: Dimensionless Kelvin-Helmholtz frequency for all the studied cases against the x/x_r. Symbols are the same as in Fig. 8. Dash line denotes a dimensionless values of 0.15.

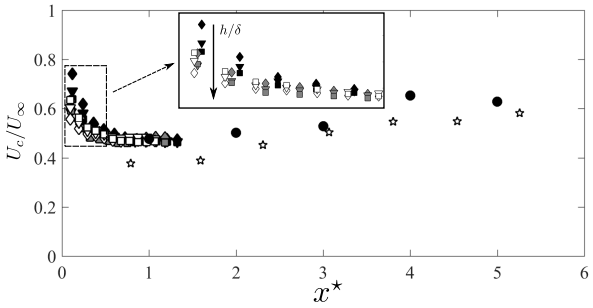

Figure 18: Evolution of convection velocity of separated flow structures on the top side against $x^\star$. ● symbol denotes the mean values corresponding to the data set from Largeau and Moriniere [19]. ☆ symbol denotes the mean values corresponding to the data set from Camussi *et al.* [5].

4. Concluding remarks

The effects of some parameters on the wall pressure statistics and on the reattachment length of a forward-facing step flow have been experimentally studied. The large-scale structures behavior evolving over the forward facing step have been analyzed. The major results are as follows:

1. The reattachment length of the first recirculation region, y_r, is slightly dependent to Reynolds number and evolves from 0.58 to 0.53 for all the studied cases in the Reynolds number range of Re_h = 110670 to 412000. The reattachment length downstream the step edge is strongly dependent of both geometrical (constriction ratio, C_R) and inflow (Re_h and h/δ ratio) parameters. A log correlation has been obtained taking into account these parameters.
2. Pressure statistic dependencies against h/δ are also highlighted. It has been shown that the mean pressure downstream the step is strongly dependent of h/δ mainly inside the recirculation area.
3. The unsteady flow investigations and especially the spectrum analysis have shown the existence of two shear-layer unsteady processes; a low frequency flapping with a dimensionless frequency, $f.x_r/U_\infty$ = 0.08 and a convective instability evolving along the separated region. The convective phenomenon, associated to the Kelvin-Helmholtz oscillation of the shear-layer, showed an asymptotic behavior and lead to the dimensionless frequency value of $f.h/U_\infty$ = 0.15 previously observed in the literature.

Acknowledgments

The present work has been supported by Campus International pour la Sécurité et l'Intermodalité des Transports, la Région Nord-Pas-de-Calais, l'Union Européenne, la Direction de la Recherche, Enseignement Supérieur, Santé et Technologies de l'Information et de la Communication et le Centre National de la Recherche Scientifique. The authors gratefully acknowledge the support of these institutions.

References

[1] **Addad Y.; Laurence D.; Talotte C.; Jacob M.C.** (1975) Large Eddy Simulation of a forward-backward facing step for acoustic source identification. Int. Journal of Heat and Fluid Flow. **24**, 1269-1276.

[2] **Awasthi M.; Devenport J.; Glegg S.A.L.; Forest J.B.** (2014) Pressure fluctuations produced by forward steps immersed in a turbulent boundary layer. Journal of Fluid Mechanics. **756**, 384-421.

[3] **Barbosa-Saldana J.G.; Morales-Contreras O.A.; Jimenez-Bernal J.A.; Gutierrez-Torres C.D.C; Moreno Pacheca L.A.** (2013) Numerical and experimental results for flow through a forward facing step channel. IJRRAS. **15(2)**, 177-189.

[4] **Bergeles G.; Athanassiadis N.** (1983) The flow past a surface-mounted obstacle. Journal of Fluids Engineering. **105**, 461-463.

[5] **Camussi R.; Felli M.; Pereira F.; Aloisio G.; Di Marco A.** (2008) Statistical properties of wall pressure fluctuations over a forward facing-step. Phy. of Fluids. **20**, 075-113.

[6] **Castro I.** (1979) Relaxing wakes behind surface-mounted obstacles in rough wall boundary layer. Journal of Fluid Mechanics. **93**, 631-659.

[7] **Castro I.; Dianat M.** (1983) Surface flow patterns on rectangular bodies in thick boundary layer. Journal of Wind Engineering and Industrial Aerodyamics. **11**, 107-119.

[8] **Cherry N.J.; Hillier R.; Latour M.E.** (1985) Unsteady measurements in a separated and reattaching flow. Journal of Fluid Mechanics. **144**, 13-46.

[9] **Fadla F.; Graziani A.; Kerherve F.; Mathis R.; Lippert M.; Uystepruyst D.; Keirsbulck L.** (2016) Electrochemical Measurements for Real-Time Stochastic Reconstruction of Large-Scale Dynamics of a Separated Flow. Journal of Fluids Engineering **138**, 121204.

[10] **Farabee M.; Casarella M.J.** (1986) Measurements of fluctuating wall pressure for separated/reattached boundary layer flows. ASME J. Vib., Acoust., Stress, Reliab. Des. **108**, 301.

[11] **Gasset N.; Poitras G.; Gagnon Y.; Brothers C.** (2005) Study of atmospheric boundary layer flows over a coastal cliff. Int. Journal of Wind Engineering **29(1)**, 3–24.

[12] **Hattori H.; Nagano Y.** (2010) Investigation of turbulent boundary layer over forward-facing step via direct numerical simulation. International Journal of Heat and Fluid Flow. **31**, 284-294.

[13] **Hudy L.M.; Naguib A.; Humphreys W.M.** (2007) Stochastic estimation of a separated-flow field using wall-pressure-array measurements. Phys Fluids **19**: 024103

[14] **Iftekhar H.; Agelin-Chaab M.** (2016) Structure of Turbulent Flows Over Forward Facing Steps With Adverse Pressure Gradient. Journal of Fluids Engineering **138**, 111202-1.

[15] **Ji M.; Wang M.** (2012) Surface pressure fluctuations on steps immersed in turbulent boundary layers. Journal of Fluid Mechanics. **712**, 471-504.

[16] **Keirsbulck L.; Fourrié G.; Labraga L.; Gad-el-Hak M.** (2012) Scaling of statistics in wall-bounded turbulent flows. Comptes rendus Mécanique. **340(6)**, 420-433.

[17] **Kiya M.; Sasaki K.** (1985) Structure of large scale vortices and unsteady reverse flow in the reattaching zone of a turbulent separation bubble. Journal of Fluid Mechanics. **154**, 463-491.

[18] **Lanzerstorfer D.; Kuhlmann H.C.** (2011) Three-dimensional instability of the flow over a forward-facing step. Journal of Fluid Mechanics. **695**, 390-404.

[19] **Largeau J.; Moriniere V.** (2007) Wall pressure fluctuations and topology in separated flows over a forward facing step. Exp. in Fluids. **42**, 21-40.

[20] **Leclercq D.; Jaob M.; Louisot A.; Talotte C.** (2001) Forward-Backward facing step pair: aerodynamic flow wall pressue and acoustic characterisation. Proceedings of the Seventh AIAA/CEAS Aeroacoustics Conference. **1249**, 075113-1-075113-13.

[21] **Marino L.; Luchini P.** (2009) Adjoint analysis of the flow over a forward-facing step. Theor. Comput. Fluid Dyn. **23**, 37-54.

[22] **Menfoukh L.; Keirsbulck L.; Mekadem M.; Oualli H.; Hanchi S.; Labraga L.;**, (2010) Near-wake aerodynamic characteristics of a radially deforming circular cylinder using LDV measurements.International Journal of Heat and Fluid Flow. **31**, 561-568.

[23] **Moss W.; Baker S.**, (1980) Re-circulating flows associated with two-dimensional steps. Aeronautical Quarterly (August), 151-172.

[24] **Sherry M.; Lo Jacono D.; Sheridan J.; Mathis R.; Marusic I.** (2009) Flow separation characterisation of a forward facing step immersed in a turbulent boundary layer. Proceedings of the Sixth International Symposium on Turbulence and Shear Flow Phenomena. **6**, 1325-1330.

[25] **Sherry M.; Lo Jacono D.; Sheridan J.** (2010) An experimental investigation of the recirculation zone formed downstream of a forward facing step. Journal of Wind Engineering and Industrial Aerodynamics. **98**, 888-894.

[26] **Ster H.; Gyr A.; Kinzelbach W.** (1999) Laminar separation on a forward facin step. European Journal of Mechanics - B/Fluids. **18**, 675-692.

[27] **Tenaud C.; Fraigneau Y.; Daru V.** (2011) Numerical simulation of the turbulent separation reattachment flow around a thick flat plate. Journal of Physics: Conference series, **318**, 1-10.